UNIVERSITÀ DEGLI STUDI DI PADOVA

Dipartimento di Fisica e Astronomia "Galileo Galilei"

Corso di Laurea in Fisica

Tesi di Laurea

Study and development of an RF buncher for SPES cyclotron at Laboratori Nazionali di Legnaro

Relatore

Prof. Marco Mazzocco

Correlatori

Dr. Mario Maggiore

Dr. Piergiorgio Antonini

Laureando

Lorenzo Buriola

Anno Accademico 2019/2020

Desidero ringraziare il Dr. Maggiore e il Dr. Antonini per l'opportunità offertami e per l'apporto e il sostegno durante il periodo stimolante di lavoro con loro.
Un sentito grazie anche al Prof. Mazzocco per la grande disponibilità e gentilezza.

Abstract

The new SPES cyclotron at Laboratori Nazionali di Legnaro is operative since 2017. In order to improve its performances, an axial Radiofrequency (RF) buncher has been studied to optimize the injection process. To achieve satisfying results, it is necessary to understand the theory of RF buncher and its effect on the injected beam. It is also necessary to run beam simulations verifying the behaviour of the system.
After introducing the SPES cyclotron and facility, an excursus on the fundamental concept of emittance is presented because of the importance that it has in beam characterization. Then, the injection line of the cyclotron will be analysed in all its major components. In order to simulate the line, each component has been reconstructed using SIMION, a software able to calculate electromagnetic fields and motion of charged particles.
The main part of the work is dedicated to the study of the buncher. At first, the general linear theory is exposed, presenting the basic function of the tool and computing the specific quantities. Then the harmonic double gap buncher is described as this is the choice adopted. Double gap allows to halve the needed voltage and harmonic waveforms are the easiest to produce. After the calculation of the optimal potential, some important corrections to the theoretical estimate are given in the so-called *Transit Time Factor*. For what concerns the design, two different layouts are studied and compared: the $\beta\lambda/2$ buncher and the $\frac{3}{2}\beta\lambda$.
Finally, in the last part, the results of multi-particle tracking done by SIMION code are reported. In this section, both transverse and longitudinal components of motion are studied, verifying the effect of the buncher inserted in the injection line and the effective current gain of the system.

Il nuovo ciclotrone del progetto SPES ai Laboratori Nazionali di Legnaro è operativo dal 2017. Allo scopo di migliorarne le prestazioni è stato studiato un buncher a Radiofrequenza (RF) per ottimizzare il processo di iniezione. Per ottenere risultati soddisfacenti è necessario comprendere la teoria del buncher e i suoi effetti sul fascio iniettato. È anche necessario simulare il sistema, verificando il suo comportamento.
Dopo aver introdotto il ciclotrone e la facility di SPES, sarà presentato un excursus sul concetto fondamentale di emittanza, per la sua importanza nella caratterizzazzione dei fasci. In seguito, verrà analizzata la linea di iniezione del ciclotrone nei suoi maggiori costituenti. Per poter simulare la linea, ognuno di essi è stato ricostruito usando SIMION, un software per il calcolo di campi elettromagnetici e del moto di particelle cariche.
La parte principale del lavoro è dedicata allo studio del buncher. Nella prima parte si espone la teoria generale, la funzione del dispositivo e i calcoli delle grandezze specifiche. Poi, l'attenzione verrà concentrata sul buncher armonico a doppio gap, in quanto questo è il layout finale adottato. Il doppio gap, infatti, permette di dimezzare il potenziale necessario e le funzioni d'onda armoniche sono le più facili da generare. Dopo il computo del voltaggio ottimale, verrano riportate delle importanti correzioni alla stima ideale nel cosiddetto Fattore di Transito*. Per quanto riguarda il design, saranno presentati e confrontati due diversi layout ($\beta\lambda/2$ e $\frac{3}{2}\beta\lambda$).*
Infine, nell'ultima parte, sono esposti i risultati delle simulazioni in SIMION. In questa sezione verranno analizzate le componenti trasversali e longitudinale del moto degli ioni, andando a verificare l'effetto dell'inserimento del buncher e l'effettivo guadagno in corrente del sistema.

Contents

1 Introduction

This work was born after the collaboration with Dr. Mario Maggiore and Dr. Piergiorgio Antonini that started in Summer 2019 thanks to a stage at Laboratori Nazionali di Legnaro. Dr. Maggiore and Antonini's group is responsible for the new high-power cyclotron at LNL, operational since 2017, which is one of the most powerful cyclotrons in Europe with its 70 MeV of energy and 700 µA of current. Its purpose is to accelerate proton beams that will be used in SPES (Selective Production of Exotic Species) project, now in development. During that experience, I have learned the basic concepts of accelerator physics and beam dynamics and I started using SIMION software in order to simulate the motion of charged particles in electromagnetic fields. In this framework, I was introduced to some issues regarding the cyclotron, in particular the study and development of a buncher that could possibly be realized and installed along the injection line in the future.

1.1 Motivations

A buncher system can be installed to improve the efficiency of the injection of a cyclotron, increasing the number of charged particles injected into the central region of the cyclotron and finally accelerated and extracted, by keeping constant the beam current extracted from the ion source. At present, the LNL cyclotron is able to achieve the current required by SPES experiments, however, a buncher can be developed for at least three reasons (see also [1]):

1) To study high current cyclotron beam dynamics and current limits
2) To achieve the needed current injecting less current from the ion source, in order to preserve the latter.
3) To increase the average current extracted from the cyclotron.

As said, in this case, no more current is needed for SPES facility, however, the study of cyclotron current limits can be relevant to verify the theoretical expectations for intensity limitations in compact cyclotrons (see [2]). Knowing the limits of the specific machine is also important for future development. The second reason is, for the technical point of view, the most important, to improve the reliability of the source by keeping low its performance in terms of extracted beam current.

1.2 Cyclotron generalities

For a detailed treatment of this topic see [3]. A cyclotron is a circular accelerator for charged particles. A charged beam injected into the machine is turned in circular orbits by a strong, almost constant, magnetic field, while two RF cavities provide acceleration to the particles. The result is a spiralling out orbit from the centre of the cyclotron to the extractor at the edge. The key point of the acceleration principle of the cyclotron is the fact that the period of a full turn is not a function of particle velocity. That is obviously true for non-relativistic energies, for which the period of particles is well known: $T = \frac{2\pi m}{qB}$. For relativistic particles, whose period depends on their speed, isochronous orbits can be obtained varying the magnetic field as incrementing radius to compensate

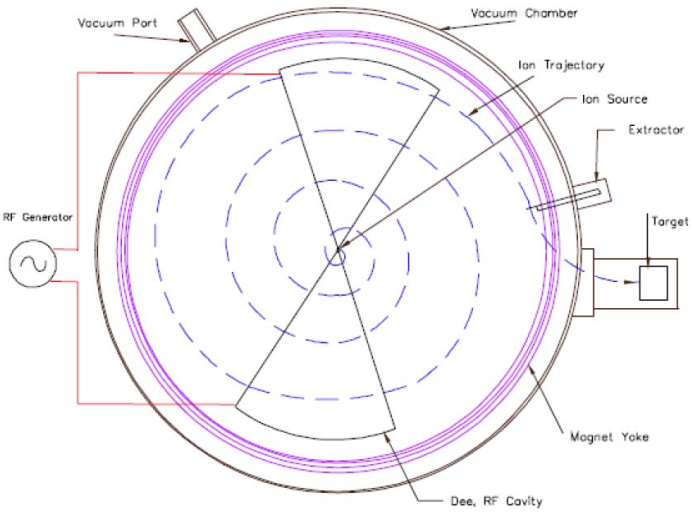

Figure 1: Scheme of the cyclotron

the relativistic increase of mass. All things considered, in isochronous cyclotrons, every bunch that composes the beam arrives at the RF gaps always at the same time, receiving every turn the same acceleration kick and getting faster and faster until reaching the extractor. RF cavities are driven sinusoidally with a frequency that is equal to or a multiple of the cyclotron frequency $\omega_{cyc} = \frac{qB}{m}$. The phase gap that cavities accelerate efficiently is called acceptance. Only particles travelling within this gap, which feel enough potential difference, are boosted correctly until the extractor.

1.3 SPES cyclotron and facility

The detailed description of SPES cyclotron and facility can be found in [4], [5], [6], [7] and [8].
The SPES facility is under construction at Laboratori Nazionali di Legnaro and first Radioactive Ion Beams are expected to be available in 2022. The purpose of SPES project is to perform research in nuclear structure, reaction dynamics and interdisciplinary fields like medical, biological and material science using high-intensity and high-quality beams of neutron-rich nuclei produced with ISOL (isotope separator on-line) technique.

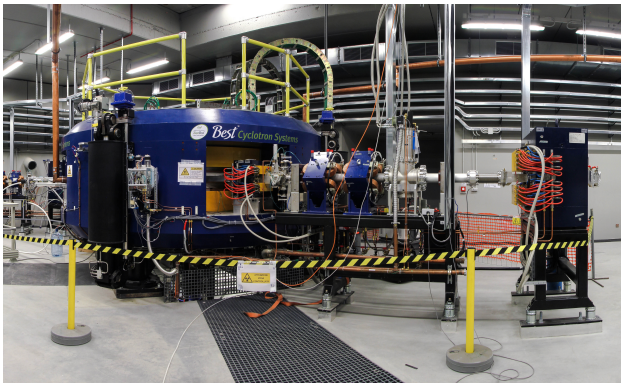

Figure 2: Photo of the cyclotron B70

The initial proton beam is supplied by the cyclotron B70 (in Fig. 2), a four sectors compact RF cyclotron with axial injection. H^- ions, provided by an ion source with a multi-cusp configuration, are accelerated by the cyclotron up to the energy of 70 MeV. Proton beams are extracted by stripping the two electrons of H^- beam passing through a thin graphite foil, to obtain H^+. There are two different extraction channels, placed at 180° one with respect to the other; that means two different beams can be produced simultaneously and can be used for two different experiments.
The cyclotron has two RF cavities operating at the frequency of $\nu = 56.16$ MHz. The phase acceptance of the machine is about $40° \div 50°$.

Parameter	Description
Cyclotron type	Compact, resistive magnet
Sectors number	4 straight sectors
Accelerated particles	H^- (proton extracted)
Beam energy range	$35 \div 70$ MeV
Beam current range	50 nA $\div$750 µA
Magnetic field at centre	1 T
Peak magnetic field	1.6 T
Pole radius	135 cm
Weight	$\sim$ 200 ton
RF system	2 delta-cavities $\lambda/2$
RF frequency	56.16 MHz, harmonic = 4
Extraction system	Stripping process
Injection system	Axial from external IS
Ion Source (IS)	Volumetric multi-cusp
Nominal intensity IS	$6 \div 10$ mA
Voltage IS	40 kV

Table 1: Cyclotron parameters, from [4].

1.4 Buncher preliminary considerations

As said in Section 1.2, cyclotron cavities accelerate efficiently only particles within a certain phase acceptance. However, the injected current produced by ion source is continuous. This means that correctly accelerated particles are only a quite small fraction, in particular, the cyclotron accelerates only $\frac{40°}{360°} \simeq 11\%$ of the beam. A buncher is used to increase the number of ions within the phase acceptance. It works as a longitudinal lens, accelerating particles, within an RF period, that would arrive late to the acceptance window and decelerating particles that would arrive too early in order to create a pulsed beam from a continuous one (see Fig. 3).

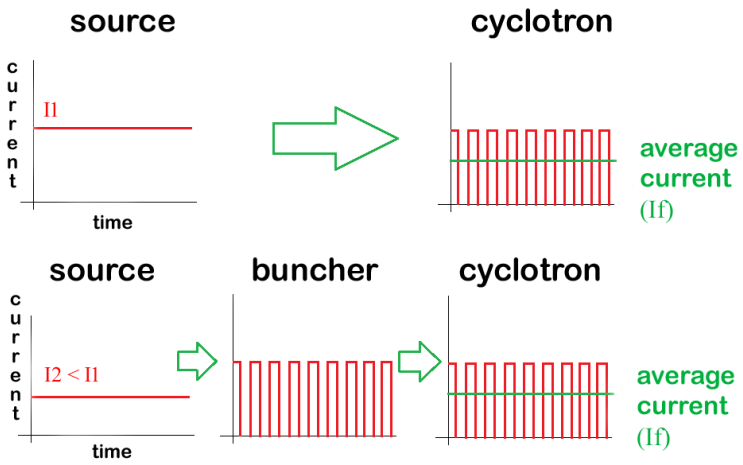

Figure 3: Scheme of buncher effect, here it is underlined how a buncher allows reducing the input current keeping unchanged the resultant one.

The effect of a buncher is to increase the injected current and consequently the average current extracted from the accelerator. Studying the characteristics of the buncher and the injection line, it is possible to maximise the bunching factor and so the number of particles within the phase acceptance.
Note that in this work the buncher will be studied from the beam dynamics point of view neglecting space charge effect (see [9]). Mechanical and electronic considerations are omitted.

2 Emittance

2.1 Definition

Here the concept of emittance is introduced because of the importance that it will have in the following chapters, for more details see [11] and [12].
The emittance is a beam property that gives an idea of its size in the phase space of the particles. The phase space variables for the beam are the canonical six coordinates (x, p_x, y, p_y, z, p_z) where x and y are the transverse coordinates, while z follows the motion of the particles. The beam is characterised by a distribution function $\varrho(x, p_x, y, p_y, z, p_z, t)$. Emittance is related to the beam volume in the phase space. In particular, in beam dynamics, we define horizontal emittance (ε_x), vertical emittance (ε_y) and longitudinal emittance (ε_z), which measure the projections of the distribution function ϱ to the coordinate-momentum plane. However, instead of canonical coordinates, normally emittance is defined using geometrical ones: $(x, x', y, y', l, \delta)$ (see [10] and [13]) where:

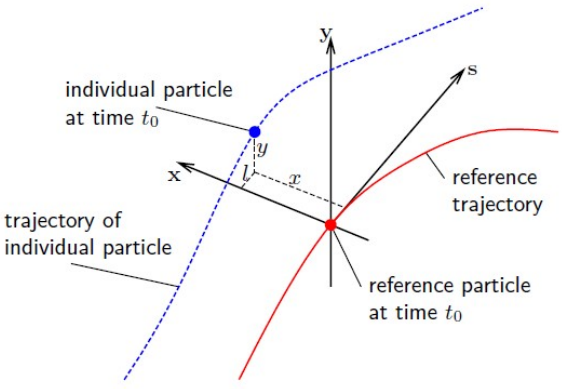

Figure 4: Scheme of used coordinates, from [10]

- x is the horizontal displacement from the reference trajectory ($x = 0$).
- x' is the horizontal slope $\frac{dx}{ds} = \frac{v_x}{v_z} \simeq \frac{v_x}{v}$, where s is in direction of motion (in our case $s \equiv z$).

- y is the vertical displacement from the reference trajectory ($y = 0$).
- y' is the vertical slope $\frac{dy}{ds} = \frac{v_y}{v_z} \simeq \frac{v_y}{v}$.
- l is the longitudinal position of the particle (in our case along z), it can be substituted by phase.
- $\delta = \frac{\Delta p}{p_0}$, where p_0 is reference momentum (generally the average), is the relative momentum deviation.

Let us consider now only transverse motion. The transverse emittance is defined considering that transverse motion on one coordinate of a single particle in a stable beam can be described using 1D Hill's equation (a complete treatment can be found in [11]).

$$x(s) = A\sqrt{\beta(s)}\cos(\psi(s)) \tag{1}$$

Where s is, as usual, the coordinate along the direction of the motion, A is the amplitude (depending on initial conditions) and β is one of the so-called *Twiss parameters*. This shows how, in a stable beam, the motion of single particle is limited. Differentiating Eq. 1 we find:

$$\alpha(s)x(s) + \beta(s)x'(s) = -A\sqrt{\beta(s)}\sin(\psi(s)) \tag{2}$$

where we introduce another Twiss parameter $\alpha = -\frac{1}{2}\frac{d\beta}{ds}$. Combining Eq. 1 and Eq. 2 we obtain:

$$\gamma x^2 + 2\alpha x x' + \beta x'^2 = A^2 \tag{3}$$

where $\gamma = \frac{1+\alpha^2}{\beta}$ is the third Twiss parameter. This is the equation of an ellipse of area πA^2 in the plane (x, x'). Coming back to Eq. 1, we can choose A in a way that the single particle amplitude $A\sqrt{\beta}$ is equal to the standard deviation of particle position in the beam (this is the typical choice) and thus define the emittance ε as the area of the given ellipse:

$$\varepsilon = \pi A^2 \quad (A\sqrt{\beta} = \sigma_x). \tag{4}$$

2.2 Statistical definition

Despite the previous definition of emittance based on particle dynamics within the beam, it is important to give another definition because of the usefulness that it has when we work with simulations. Following what presented in [14], the statistical definition of emittance is based only on the distribution of particles in phase space. In x, y, x', y' coordinates beam is usually distributed as a multivariate normal distribution.

$$f(\mathbf{x}) = \frac{1}{(2\pi)^2|\mathbf{\Sigma}|^{\frac{1}{2}}} e^{-\frac{(\mathbf{x}-\mu)^T\mathbf{\Sigma}^{-1}(\mathbf{x}-\mu)}{2}} \tag{5}$$

where $\mathbf{x}$ is a 4-dimensional vector, μ is the 4-dimensional mean vector and $\mathbf{\Sigma}$ is the covariance matrix that, in this case, is also called beam matrix.

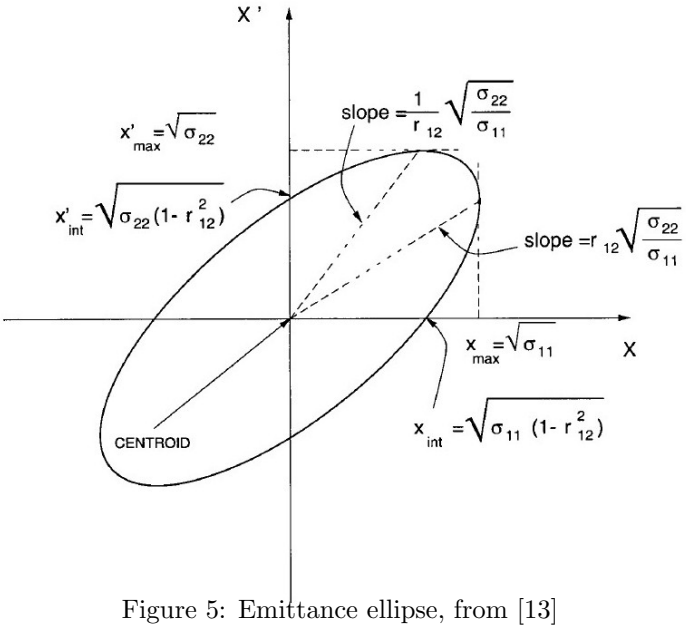

Figure 5: Emittance ellipse, from [13]

The projections on (x, x') and (y, y') planes of the distribution in Eq. 5 are bivariate normal with elliptical constant density contours. Now we define the transverse emittance as the area of the ellipse that contains a certain fraction of particles. Given the fraction p it is well known that the ellipse that we find is described by the equation (in plane (x, x')):

$$\begin{bmatrix} x & x' \end{bmatrix} \begin{bmatrix} \sigma_{11} & \sigma_{12} \\ \sigma_{21} & \sigma_{22} \end{bmatrix}^{-1} \begin{bmatrix} x \\ x' \end{bmatrix} = \chi_2^2(p) \tag{6}$$

where $\chi_2^2(p)$ is the chi-square function with 2 degree of freedom and the inverse of the (x, x') covariance matrix appears. The semi axes of the ellipses are given by the eigenvalues $(\lambda_1,\ \lambda_2)$ of the covariance matrix. In particular they are equal to $\sqrt{\chi_2^2(p)\lambda_i}$ $(i = 1, 2)$.

$$\lambda_{1,2} = \frac{\sigma_{11} + \sigma_{22} \pm \sqrt{(\sigma_{11} - \sigma_{22})^2 + 4\sigma_{12}^2}}{2}$$

The area of the ellipse, that is the emittance is:

$$\varepsilon_p = \pi\chi_2^2(p)\sqrt{\lambda_1\lambda_2} = \pi\chi_2^2(p)\sqrt{\frac{1}{4}\left[(\sigma_{11} + \sigma_{22})^2 - (\sigma_{11} - \sigma_{22})^2 + 4\sigma_{12}^2\right]} = \pi\chi_2^2(p)\sqrt{\sigma_{11}\sigma_{22} - \sigma_{12}^2}$$

We can rewrite the result:

$$\varepsilon_p = \pi\chi_2^2(p)\sqrt{\begin{vmatrix} \sigma_{11} & \sigma_{12} \\ \sigma_{21} & \sigma_{22} \end{vmatrix}} = \pi\chi_2^2(p)\sigma_x\sigma_{x'}\sqrt{1 - \rho^2} \tag{7}$$

In Eq. 7 we outline the dependence on the standard deviation of the single coordinate and the correlation coefficient $\rho = \frac{\sigma_{12}}{\sqrt{\sigma_{11}\sigma_{22}}}$. In the next pages we will indicate with ε the value $\pi\sigma_x\sigma_{x'}\sqrt{1 - \rho^2}$, while with ε_p we denote the emittance containing a fraction p of particle, note that $\varepsilon_p = \chi_2^2(p)\varepsilon$.

Eq. 6 can be rewritten as

$$\frac{1}{\sigma_{11}\sigma_{22} - \sigma_{12}^2}(\sigma_{22}x^2 - 2\sigma_{12}x'x + \sigma_{11})x'^2) = \chi_2^2(p)$$

Comparing with the ellipses in Eq. 3 it is easy to see that *Twiss parameters* can be written as:

$$\alpha = -\frac{\pi\rho\sigma_x\sigma_{x'}}{\varepsilon}; \qquad \beta = \frac{\pi\sigma_x^2}{\varepsilon}; \qquad \gamma = \frac{\pi\sigma_{x'}^2}{\varepsilon} \tag{8}$$

2.3 Emittance conservation

Thanks to Liouville theorem we know that, if the system is conservative, the beam volume in the phase space is invariant. If the coupling among the three coordinates is weak, we can treat the motion in each plane separately. In this case, every volume projection on coordinates (x, p_x) plane is invariant. However, emittances are calculated on (x, x') planes. The relation between momenta and slopes is the following:

$$p_x = m\beta\gamma cx' \tag{9}$$

where m is the mass of the particle, c is the speed of light, $\beta = \frac{v}{c}$, $\gamma = 1/\sqrt{1-\beta^2}$. So, the emittance in each plane is invariant only if $\beta\gamma$ is constant, which means there is no acceleration. However, we can define an invariant constant called normalized emittance that does not depends on speed variations:

$$\varepsilon_{norm} = \varepsilon\beta\gamma \tag{10}$$

Unfortunately, in the cyclotron injection line, that will be studied in the next pages, the presence of solenoids produce coupling between the transversal coordinates, so the emittances on x and y are not invariant. For what concerns the longitudinal motion, we will not calculate emittance (that is not invariant because of the introduction of the buncher) but we will give the energy dispersion and the phase distribution of particle within the beam.

3 The injection line: state of art

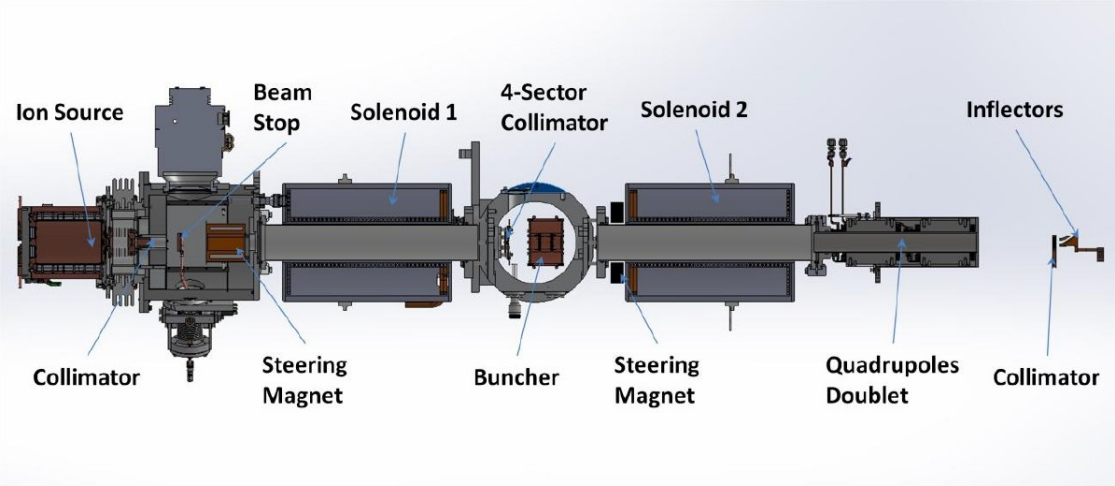

Figure 6: Scheme of the present injection line with the insertion of a buncher (courtesy by Best Theratronics).

The SPES cyclotron has an axial injection line located underneath the machine itself. It is about 2.3 meters long and it is designed to transport the beam from the source to the cyclotron inflector with minimum beam losses. Different solutions were studied but the final one consists of a couple of solenoids, a couple of quadrupoles, a collimator and two steerers (Fig. 6). The dimensions of every component are shown in Tab. 2. Some injection line details are taken from [15]

Element	Distance from IS [mm]	Length [mm]	Aperture [mm]
Solenoid-1	353	411	85
Solenoid-2	1195	411	85
Quadrupole-1	1730	120	50
Quadrupole-2	1910	120	50
Inflector	2232	-	-

Table 2: Dimensions and locations of the main compounds of the injection line

The injection line was partially reproduced with software SIMION in order to simulate its behaviour with and without the insertion of the buncher system. In the following sections there are some comments on every component of the line.

3.1 Ion Source

The source is a H^- multi-cusp type, designed to produce up to a 10 mA ion beam. It is composed by a plasma chamber with a strong magnetic confinement. Ten columns of permanent magnets with alternating north and south poles produce a field that traps ions preventing losses through collisions with walls. H^- are produced by process in Eq. 11, by an electron attachment to vibrational excited hydrogen molecules in the plasma volume.

$$e^- + H_2^* \rightarrow H_2^{-*} \rightarrow H^- + H \tag{11}$$

The extraction system is composed by two pairs of small permanent magnets for electron filtration and electrodes that accelerate ions to the energy of $E = (40000 \pm 1)$ eV.

Other information about the multi-cusp ion source can be found in [6], [8], [16] and [17]

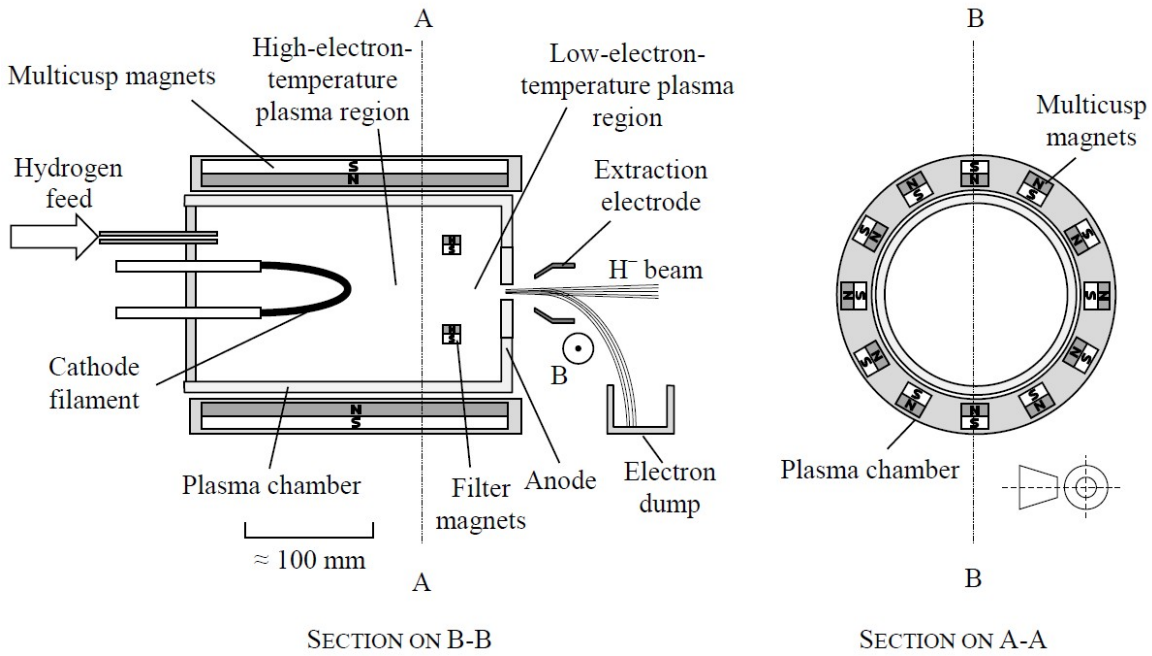

Figure 7: Scheme of the Ion Source

Transverse beam characteristics at the exit of the ion source are measured using an Allison scanner, able to perform emittance tests (see [18]), located at a distance of 155 mm downstream of the ion source ground electrode. The results of measurement are reported in Tab. 3. In the table the covariance matrix elements, the emittance, the maximum positions and slopes of particles and the correlation coefficients are shown.

	2 mA		4 mA		6 mA	
Axis	X	Y	X	Y	X	Y
σ_{11} [mm^2]	70.515	56.313	43.28	53.394	42.418	56.987
σ_{12} [mm·mrad]	309.925	247.192	213.542	224.322	208.867	243.471
σ_{22} [mrad^2]	1385.28	1110.81	1082.57	991.611	1072.651	1102.666
Beam%	89.98	89.92	89.99	89.98	90.00	89.95
ε [π·mm·mrad]	40.367	38.0625	35.044	51.246	43.289	59.6617
ε_{norm} [π·mm·mrad]	0.3726	0.3513	0.3235	0.4730	0.3996	0.5507
X_{max} [mm]	8.397	7.504	6.579	7.307	6.513	7.549
X'_{max} [mrad]	37.219	33.329	32.902	31.490	32.751	33.206
ρ	0.9916	0.9884	0.9865	0.9749	0.9792	0.9713

Table 3: Beam measurement, note that these quantities are referring the 90% of the beam.

In the simulations the ion beam is set to start from 155 mm, where the Allison scanner was located. Doing so we can use the starting parameters measured in Tab. 3 (in particular those concerning a current of 6 mA are used). The simulated transverse starting setting is visualized in Fig. 8 and in Tab. 4, where the starting parameters are reported. Note that the emittances are very similar to the one reported in Tab. 3.

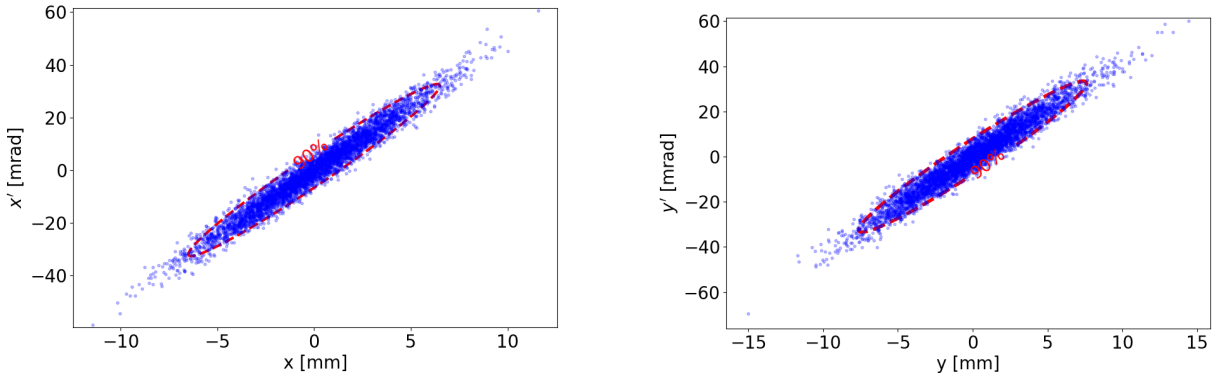

(a) *X-Emittance plot* (b) *Y-Emittance plot*

Figure 8: Emittance plots of the beam at 155 mm from the ion source

	$\varepsilon_{90\%}$ [π·mm·mrad]	α	β [mm/mrad]	γ [mrad/mm]	R_{max} [mm]	R'_{max} [mrad]
X	43.3	-4.80	0.97	24.6	6.5	32.7
Y	60.3	-4.10	0.96	18.6	7.6	33.4

Table 4: Simulated beam characteristic at 155 mm from the ion source

In order to simulate a continuous beam, particles are generated with a uniform distribution in time within a time gap of 0.02 µs, that contains a RF period $T = \frac{1}{\nu} \simeq 0.018$ µs.

3.2 Solenoids

The function of solenoids is to focus a divergent beam in both transverse directions. That happens because, while the longitudinal magnetic field does not radially deflect ions, the radial component in fringing field region at the edges of the solenoid does have a fucusing effect on the beam (for more details see [12] and [19]).

The two solenoids in the cyclotron injection line are identical. They are composed of a coil made by a square hollow copper tube and a steel shield at the external edge. The role of the first one is to focus the beam coming from the source into the chamber that contains the buncher; its axial magnetic field is about 2120 G at the centre. The second one focuses the divergent beam into the quadrupoles, here the axial magnetic field at the centre is about 1740 G.

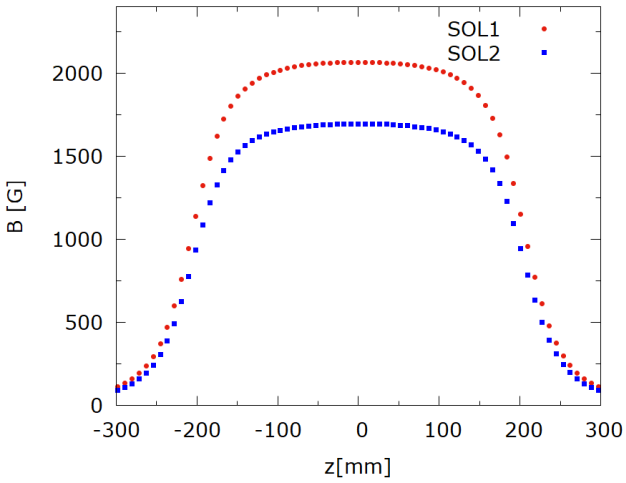

Figure 9: Solenoids axial field

In SIMION solenoids are approximated using a specific function that calculates the magnetic fields trough the Bio-Savart law. The necessary current is computed from the equation $B = \mu_0 nI$. In Fig. 9 the axial fields are reported.

3.3 Quadrupoles

It is well known that the effect of quadrupole doublets is to focus the beam in both x and y axis. In this case, the function of quadrupoles is to achieve the needed transversal beam matching at the inflector, the ending component of the injection line, whose purpose is to transport the beam into the central region of the cyclotron. The peculiarity of quadrupoles is to have a field gradient that can be considered constant over the transverse dimensions of the beam passing trough. In our case the gradients are set to 0.396 T/m for the first one and 0.650 T/m for the second one.

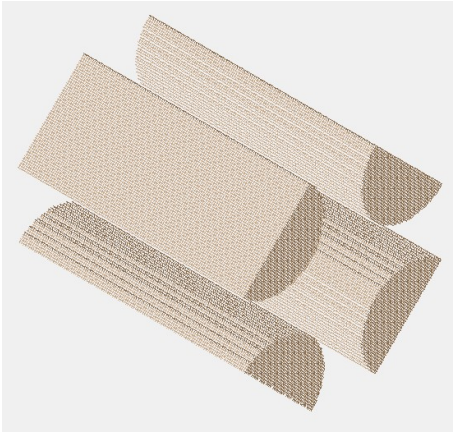

Figure 10: Quadrupole in SIMION

The software SIMION allows the definition of a scalar potential for magnetic field. The quadrupoles are simulated through the construction of four semi-cylindrical poles as can be seen in Fig. 10 and assigning to two of them a scalar potential in order to reach the needed gradient.

4 RF Buncher study

A buncher usually consists of two or three coaxial cylinders separated by gaps and on one of them is applied a variable voltage. In order to match the cyclotron phase acceptance, it must be driven with a periodic waveform with the same frequency of the cyclotron RF cavities. In Tab. 5 the parameters that will be used in the following section for the buncher studies are reported: L is the distance between the centre of the buncher and the inflector, $2\phi_{max}$ is the cyclotron acceptance.
Apart from the energy, the other quantities, presented in this table and in the next pages, are shown without their statistical error. For some of them it is negligible (the relative error is about 10^{-5}), for other the error is difficult to evaluate. However, the calculations reported in the following pages aim to give only a theoretical estimate, that will be checked with simulations. Both theory and simulations do not count some important uncertainties due to the electronics and mechanics of the line which give the main part of the statistical errors.

E	(40000 ± 1) eV
m	939 MeV
γ	1.00004
β	0.009
L	1233 mm
ν	56.16 MHz
λ	5.3 m
$2\phi_{max}$	40°

Table 5: Sum up of the most important parameters for buncher studies

4.1 Generalities

Some calculations of this Section are taken from [20]. For instance, let us now consider a one gap buncher, composed of two cylinders separated by one gap. One of those electrodes is driven with a time-variable voltage, the other is at ground. Consider particles within an RF period. The buncher purpose is to accelerate some of them and decelerate the others in order to let them arrive at the inflector at the same time in a bunch.
During their passage in the gap, particles are affected by different intensities of electric field depending on their time of arrival at the gap (or their phase), because of the voltage is varying in time. There are particles that pass the gap when $V(t) = 0$ V and are not accelerated (the so-called synchronous particles), particles that are accelerated (the late ones) and particles that are decelerated (the early ones). Synchronous particles arrive at the inflector in:

$$\tau = \frac{L}{\beta c} \tag{12}$$

Instead, an early (or late) particle, covers the distance L in:

$$\tau' = \Delta t + \frac{L}{\beta' c} \tag{13}$$

where Δt is the difference in time with the synchronous particle and β' is the new velocity after the acceleration or the deceleration passing the gap.

In order to maximise the focusing effect at the inflector τ and τ' must be the same. Under this request, combining Eq. 12 and Eq. 13 we obtain:

$$\beta' c = \frac{\beta c}{1 - \frac{\beta c}{L}\Delta t}$$

The classical (non relativistic) kinetic energy can be calculated ($\gamma \simeq 1$)

$$E' = E + \Delta E = \frac{E}{(1 - \frac{\beta c}{L}\Delta t)^2}$$

From this we can compute the needed voltage:

$$\Delta V = \frac{\Delta E}{q} = \frac{E}{q}\left(\frac{1}{(1 - \frac{\beta c}{L}\Delta t)^2} - 1\right) \approx \frac{E}{q} \cdot \frac{2\beta c}{L}\Delta t \quad \left(\frac{\beta c}{L}\Delta t \ll 1\right)$$

Note that $\Delta t \sim \frac{1}{2\nu}$, so the previous approximation is valid when the distance between the buncher and the inflector is much larger than the value $\beta\lambda/2$ (in our case $\frac{\beta\lambda}{2L} \sim 0.02$).

From the last formula we can see that the needed voltage is proportional to the delay of the particle with a proportional constant:

$$k = \frac{2E\beta c}{qL}$$

From these results we can conclude that the optimal configuration for the voltage is a sawtooth waveform with slope k. This type of wave can, in theory, bunch all particles within a phase of 2π in a single point.

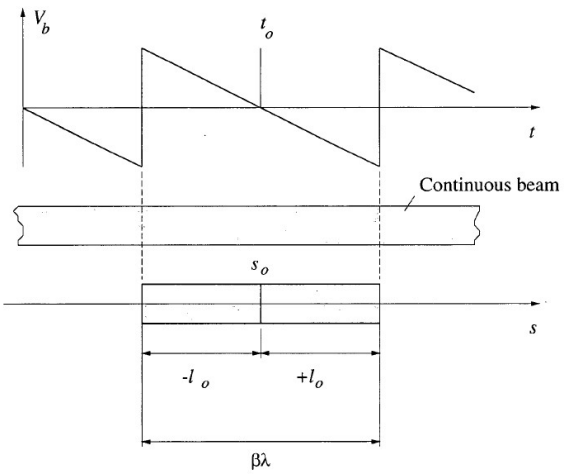

Figure 11: Linear buncher function, from [13]

Using our data: $k \simeq 1.80 \cdot 10^{11}$ V $\cdot$ s^{-1}. For a perfect bunching early and late particles within a period must be included, that implies that $V_{max} = k\frac{T}{2} = \frac{k}{2\nu} \simeq 1600$ V.

4.2 Double gap buncher

In order to halve the needed voltage, a double gap buncher can be used. It is composed of three electrodes. Those on either end are grounded, while the one in the centre is fed. The working principle of this type of buncher is shown in Fig. 12. If the distance between the two gap centres is an odd multiple of $\beta\lambda/2$ the applied voltage is used two times: a particle which is accelerated in the first gap will experience the same acceleration also in the second gap. Therefore, the amplitude of the voltage supplied to the buncher is half the required one for the one gap configuration.

For symmetry reasons a double gap buncher cannot operate with a sawtooth wave, otherwise, we have a focusing effect in the first gap but defocusing in the second. We can use a triangular wave (due to its symmetric period). This fact is a limitation for the efficiency because a sawtooth waveform, ideally, can bunch all the particles within an RF period (efficiency of 100%), while a triangular one manages to bunch particles only in half period ($\epsilon = 50\%$). Nevertheless, we will see that this is not a clear disadvantage because of the impossibilities of shaping a real sawtooth wave and the fact that we are going to use a more easily obtainable sinusoidal shape. Moreover, the presence of two grounded electrodes at the edges avoids harmful effects on beam dynamics due to the fringing field outside the buncher.

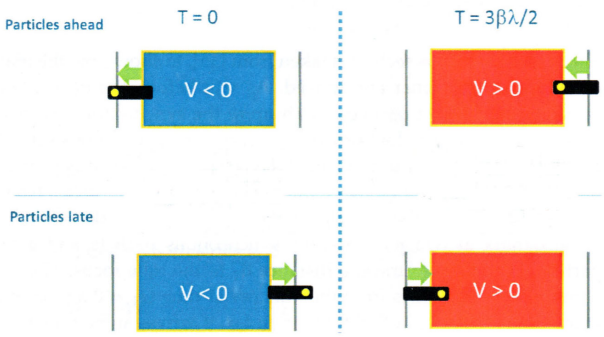

Figure 12: Working principle of a double gap buncher

4.3 Harmonic buncher

Sawtooth and triangular waveforms are technically difficult to generate. Most commonly harmonic shapes are used. The simplest one is the sinusoidal waveform, for which we can perform an analytic calculation of the needed voltage (see also [21]). Note that sawtooth or triangular waveforms can be obtained with the sum of different harmonics.
The final phase of a particle passing through the double gap buncher, whose velocity transforms from v to v', can be calculated as:

$$\phi_f = 2\pi\nu L\left(\frac{1}{v} - \frac{1}{v'}\right) = \frac{2\pi\nu L}{v}\left(1 - \sqrt{\frac{2qV(\phi_i)}{E}}\right) \simeq \phi_i - \frac{2\pi\nu L}{v}\frac{qV(\phi_i)}{E} \quad \left(\frac{qV}{E} \ll 1\right)$$

where the factor 2 inside the square root is due to the double gap. If the central electrode is driven with a sinusoidal waveform ($V(\phi_i) = V_0 \sin(\phi_i)$), we can write:

$$\phi_f = \phi_i - \mu \sin\phi_i \tag{14}$$

where $\mu = \frac{2\pi\nu L}{v}\frac{qV_0}{E}$ is called *bunching parameter*.

It is simple to demonstrate that, calling $2\phi_{max}$ the phase acceptance of the cyclotron, the maximum bunching effect is obtained when the local maximum and minimum of Eq. 14 are equal to ϕ_{max} (Fig. 14.a). Differentiating the previous equation with respect to ϕ_i and using this result we get the following relation:

$$\phi_{max} = \cos^{-1}\left(\frac{1}{\mu}\right) - \sqrt{\mu^2 - 1} \tag{15}$$

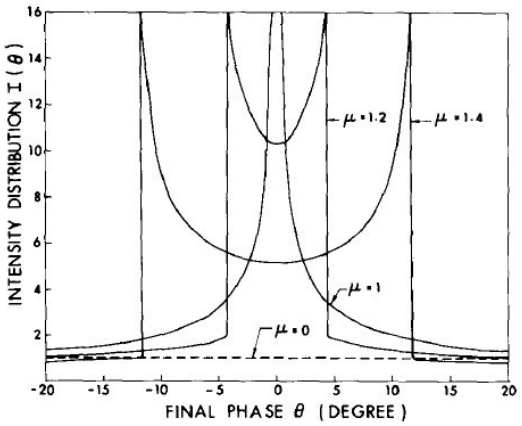

Figure 13: Phase distribution as a function of the μ parameter, from [21]

Thanks to Eq. 15 for a given acceptance, optimal μ coefficient and V_0 can be calculated. In Fig. 14.b we can see the μ coefficient as a function of the phase acceptance. For $2\phi_{max} = 40°$ we obtain $\mu \simeq 1.59$ that means we need $V_{0,ideal} \simeq 405$ V.

The μ parameter is also related to the final phase distribution of the particles as can be seen in Fig. 13. In [21] and [22] it has been calculated that for $\mu > 1$ the distribution has two symmetric maxima due to shape of the function in Fig. 14.a.

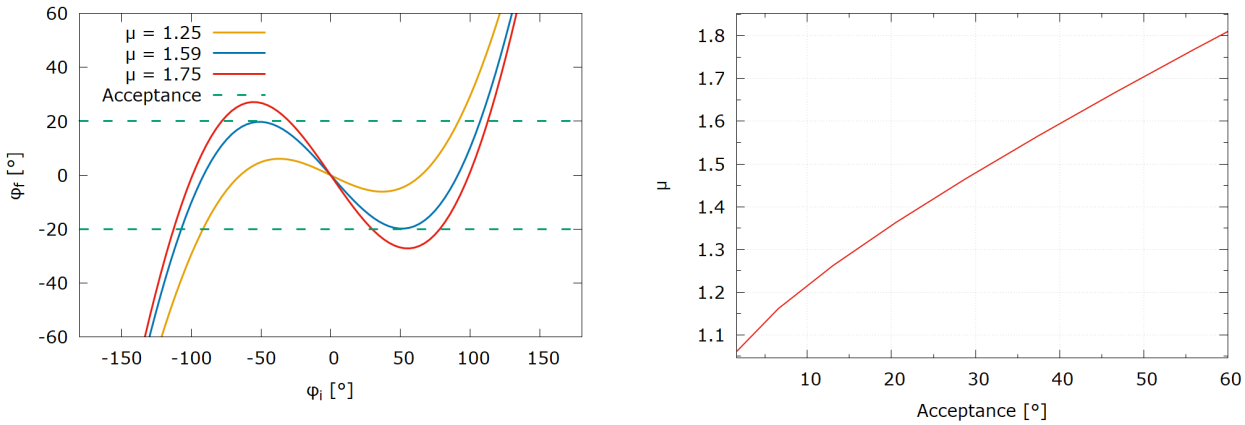

(a) *Final phase as a function of initial one*

(b) *μ coefficient as a function of phase acceptance*

Figure 14: Harmonic buncher principles

4.4 Transit Time Factor

Some corrections must be added at the previous evaluation due to the physical dimensions of cylinders and gaps. The first one comes from the fact that gaps have a finite length g, so every particle has a finite transit time t_g in the gap during which the electric field is variable. For example, a particle with a certain delay $\tilde{t}$ does not experience the ideal potential difference $\tilde{V} = V_0 \sin(2\pi\nu\tilde{t})$, but a voltage given by the mean of the function $V(t)$ in the time gap t_g:

$$\widetilde{V'} = \frac{1}{t_g}\int_{\tilde{t}-\frac{t_g}{2}}^{\tilde{t}+\frac{t_g}{2}} V_0 \sin(2\pi\nu t)dt = \frac{\beta c}{g}V_0\frac{1}{2\pi\nu}\left\{\cos\left[2\pi\nu\left(\tilde{t}-\frac{g}{2\beta c}\right)\right]-\cos\left[2\pi\nu\left(\tilde{t}+\frac{g}{2\beta c}\right)\right]\right\}=$$

$$= V_0\frac{\beta c}{2\pi\nu g}\cdot 2\sin(2\pi\nu\tilde{t})\sin\left(\frac{2\pi\nu g}{2\beta c}\right)= \widetilde{V}\frac{\sin(\frac{\pi\nu g}{\beta c})}{\frac{\pi\nu g}{\beta c}}$$

that is systematically less than the ideal one.

There is another effect that cannot be ignored. A single particle experiences different values of electric field depending on its distance from the axis of the buncher. This correction can be calculated analytically, see [23]. The total *Transit Time Factor* (TTF) that contains both these corrections is:

$$TTF = I_0(Kr)\frac{J_0(\frac{2\pi\nu a}{c})}{I_0(Ka)}\frac{sin(\frac{\pi\nu g}{\beta c})}{\frac{\pi\nu g}{\beta c}} \tag{16}$$

where r is the particle distance from axis, J_0 and I_0 are the Bessel functions, $K = \frac{2\pi\nu}{\gamma\beta c}$ and a is the internal radius of the buncher. In order to get the final needed potential we have to divide the $V_{0,ideal}$ found in Section 4.3 by the TTF.

In Fig. 15.a it is shown how the Transit Time Factor becomes more and more important as the particle is nearer to the axis. This is due to the fact that the buncher is composed by cylindrical electrodes which means that the electric field is more intense near the edges and less intense in the centre. Moreover the Transit Time Factor is very low for big radii: while a is becoming smaller, the TTF is almost 1. This suggests that the buncher should have the smallest possible radius to minimise the voltage needed (see also [24]). As expected, from Fig. 15.b we can see that small gaps are preferred. The distance g must be small enough, otherwise the bunching effect can be lost.

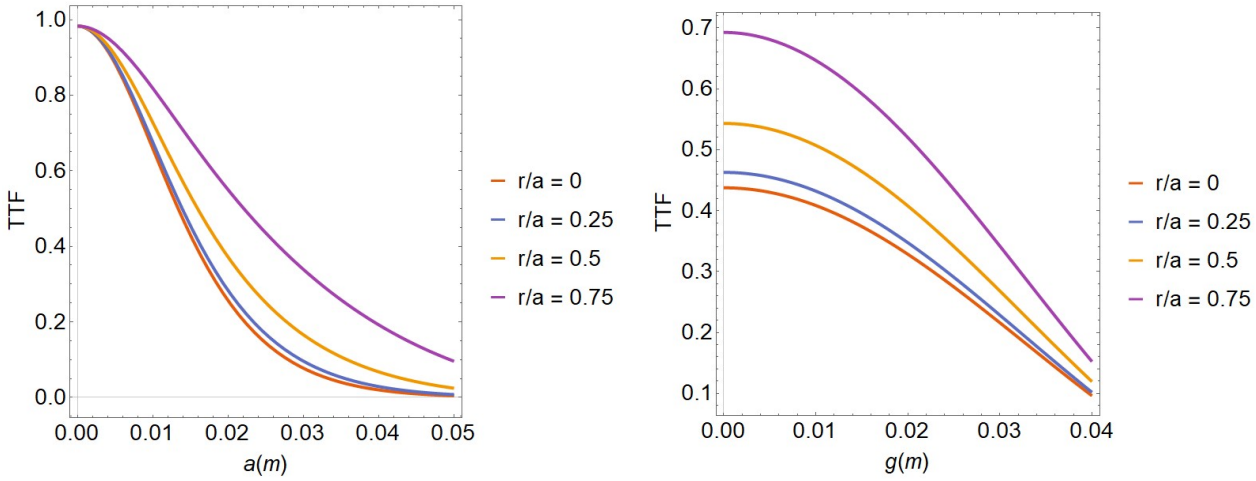

(a) *TTF as a function of the radius of the buncher*

(b) *TTF as a function of gap length*

Figure 15: TTF dependence on buncher parameters

4.5 Design considerations

In SPES cyclotron injection line, the buncher has to be inserted between the two solenoids in a dedicated chamber, with the centre of the buncher located at 999 mm from the ion source. A double gap harmonic buncher is chosen.

From simulations we can see that, in the buncher position, the beam has a maximum diameter of about 16 mm (Fig 16). Following what said in Section 4.4, to minimise the voltage needed, the minimum possible radius a must be chosen. A 20 mm diameter is permitted but it would be risky to use because the beam section is strongly correlated to the real injection parameters, such as the source current, real injection line settings and space charge effect. As a consequence the beam section might be larger, so in order to avoid any beam losses we choose to use a buncher with a 30 mm internal diameter. The length of gaps is set to 5 mm.

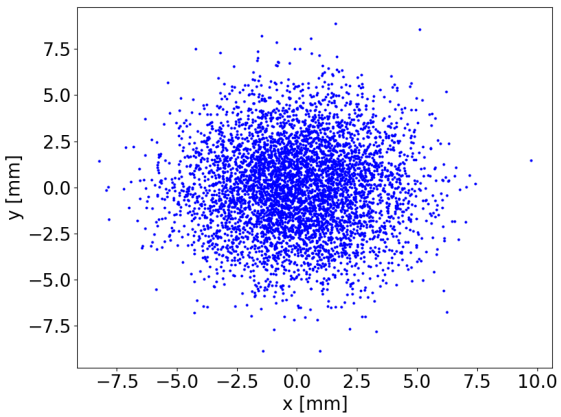

Figure 16: Maximum beam section in the buncher

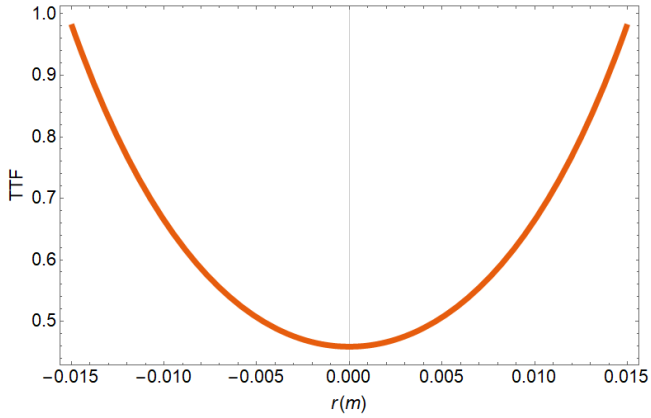

Figure 17: TTF as a function of the distance from axis

Now we can compute the needed voltage. To give an evaluation of the Transit Time Factor, we consider the average effect to the beam. In order to simplify the calculus, let us consider the beam measured in the centre of the buncher. At that point, the beam section distribution can be approximated by a 2D gaussian function where the 90% of particles are within 3.5 mm to the axis (Tab. 6).

The average TTF can be calculated:

X_{max}	3.1 mm
X'_{max}	39.8 mrad
Y_{max}	3.5 mm
Y'_{max}	36.8 mrad

Table 6: 90% beam data in the centre of the buncher (z = 999 mm)

$$\widehat{TTF} = \frac{\int_0^{2\pi} d\varphi \int_0^a TTF(r) f(r) r dr}{\int_0^{2\pi} d\varphi \int_0^a f(r) r dr} \simeq 0.47 \tag{17}$$

Where $f(r) = \frac{1}{\sqrt{2\pi}\sigma_r} e^{\frac{1}{2}\frac{r^2}{\sigma_r^2}}$ is the 1D gaussian density of probability that describes the radial distribution of the beam.

Considering all those effects, the voltage V_0 needed for an optimal bunching effect is:

$$V_0 = \frac{V_{0,ideal}}{\widehat{TTF}} \simeq 860\ V$$

Now let us focus on the electrodes. From Section 4.2 we know that the central electrode length must be an odd multiple of $\beta\lambda/2$. Because of the limited dimensions of the chamber where the buncher should be located, there are only two possible configurations that are now presented and will be compared in the following Section (see also [25] and [26]):

- $\beta\lambda/2$ buncher (Fig. 18.a), with our data $\beta\lambda/2 = 24.6$ mm. It means that the length of the central electrode is $\beta\lambda/2 - 2 \cdot \frac{g}{2} = 19.7$ mm, where g is the gap length.

Element	From [mm]	To [mm]	Length [mm]	Int.diam. [mm]	Ext. diam. [mm]
Elect-1	0	40	40	30	40
Gap	40	45	5	-	-
Elect-2	45	64.7	19.7	30	40
Gap	64.7	69.7	5	-	-
Elect-3	69.7	109.7	40	30	40

Table 7: Sizes of the $\beta\lambda/2$ buncher

- $\frac{3}{2}\beta\lambda$ buncher (Fig. 18.b), in this case $\frac{3}{2}\beta\lambda = 73.9$ mm, so the length of the central electrode is 68.9 mm.

Element	From [mm]	To [mm]	Length [mm]	Int.diam. [mm]	Ext. diam. [mm]
Elect-1	0	20	20	30	40
Gap	20	25	5	-	-
Elect-2	25	93.9	68.9	30	40
Gap	93.9	98.9	5	-	-
Elect-3	98.9	118.9	20	30	40

Table 8: Sizes of the $\frac{3}{2}\beta\lambda$ buncher

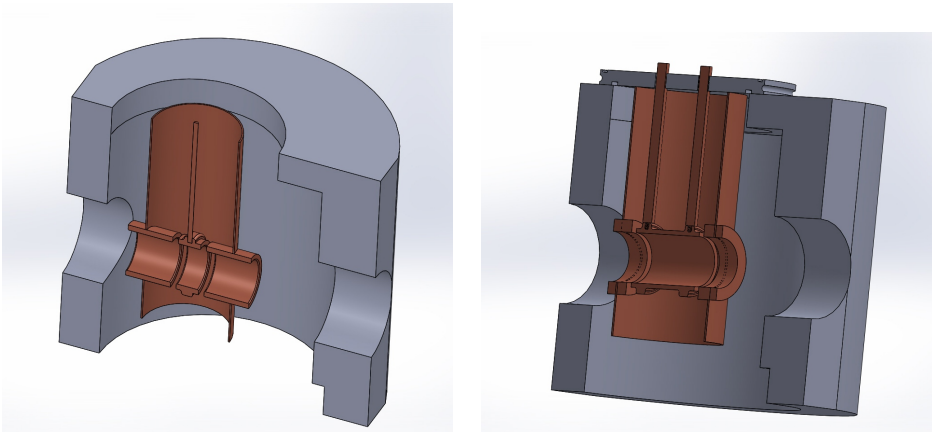

(a) *Rendering of the $\frac{1}{2}\beta\lambda$ buncher* (b) *Rendering of the $\frac{3}{2}\beta\lambda$ buncher*

Figure 18: Buncher rendering from [25]

5 Injection line simulations

In this Section, the results of simulations of the injection line with a double gap harmonic buncher inserted are reported. In SIMION a buncher can be easily simulated by modelling three coaxial cylindrical electrodes and by giving them the proper voltage (Fig. 19). Both $\beta\lambda/2$ buncher and $\frac{3}{2}\beta\lambda$ buncher are used and the design parameters chosen are those in Tab. 7 and Tab. 8. SIMION software allows measuring particles characteristics at a fixed distance from the beginning of the line. In Fig. 20 the complete simulated line is reported with the ion trajectories in blue. In Fig. 21 we report the emittance graphs for transversal and longitudinal motion at different points of the injection line underlined in orange in Fig. 20: at the Allison Scanner location (155 mm), after the first solenoid (840 mm), after the buncher (1080 mm), after the second solenoids (1700 mm) and at the inflector(2232 mm).

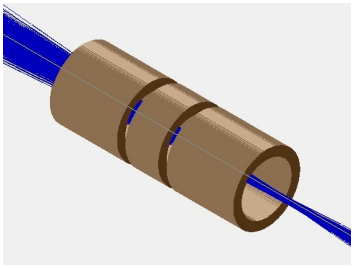

Figure 19: $\beta\lambda/2$ buncher in SIMION

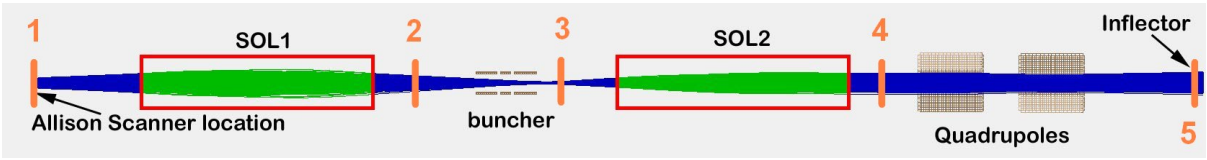

Figure 20: Injection line in SIMION

5.1 Transverse dynamics

Theoretically, a buncher does affect the transverse dynamics. Particles travelling in the gap are subjected by an electric field that is not uniform and has transverse components that can focus or defocus ions (Fig. 22). At the entrance of the gap, particles are focused, while at the exit they are defocused. The resultant effect depends on the time of flight of the single ion. Considering a harmonic buncher, particles passing through the gaps when the electric field is increasing, which are particles that will be bunched, feel a defocusing field more intense that the focusing one, so are transversal defocused. On the contrary, those passing while the electric field is decreasing are focused; however these are the particles that will be lost because not bunched.

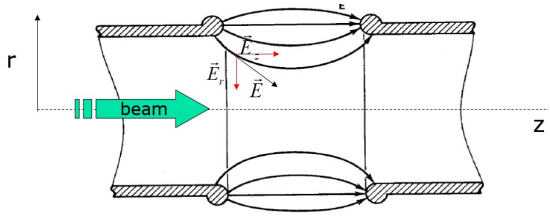

Figure 22: Electric field in an RF gap

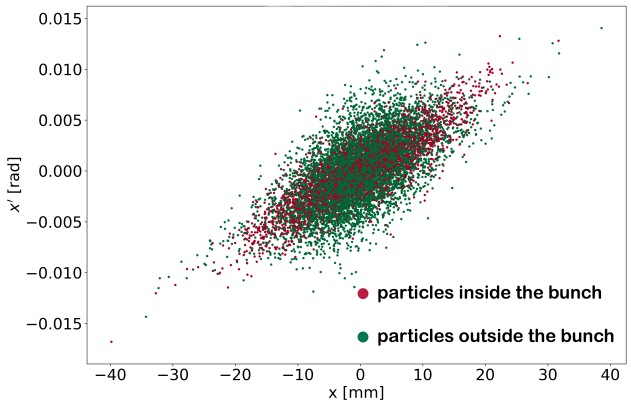

Figure 23: X-emittance of slightly defocused beam at about 1.5 m from the buncher

This effect can be easily seen for a slightly defocused beam (Fig. 23). In this case, we simulate a beam composed of identical particles with very small transverse momenta. In the simulation solenoids and quadrupole are removed and the beam fills all the buncher diameter. The transverse emittance graph shows a peculiar shape due to the overlapping of two ellipses tilted differently. The red dots are particles within the bunch while the green ones are the particle outside. See how bunched ions are distributed in a more tilted ellipse which means they are much more defocused than the others.

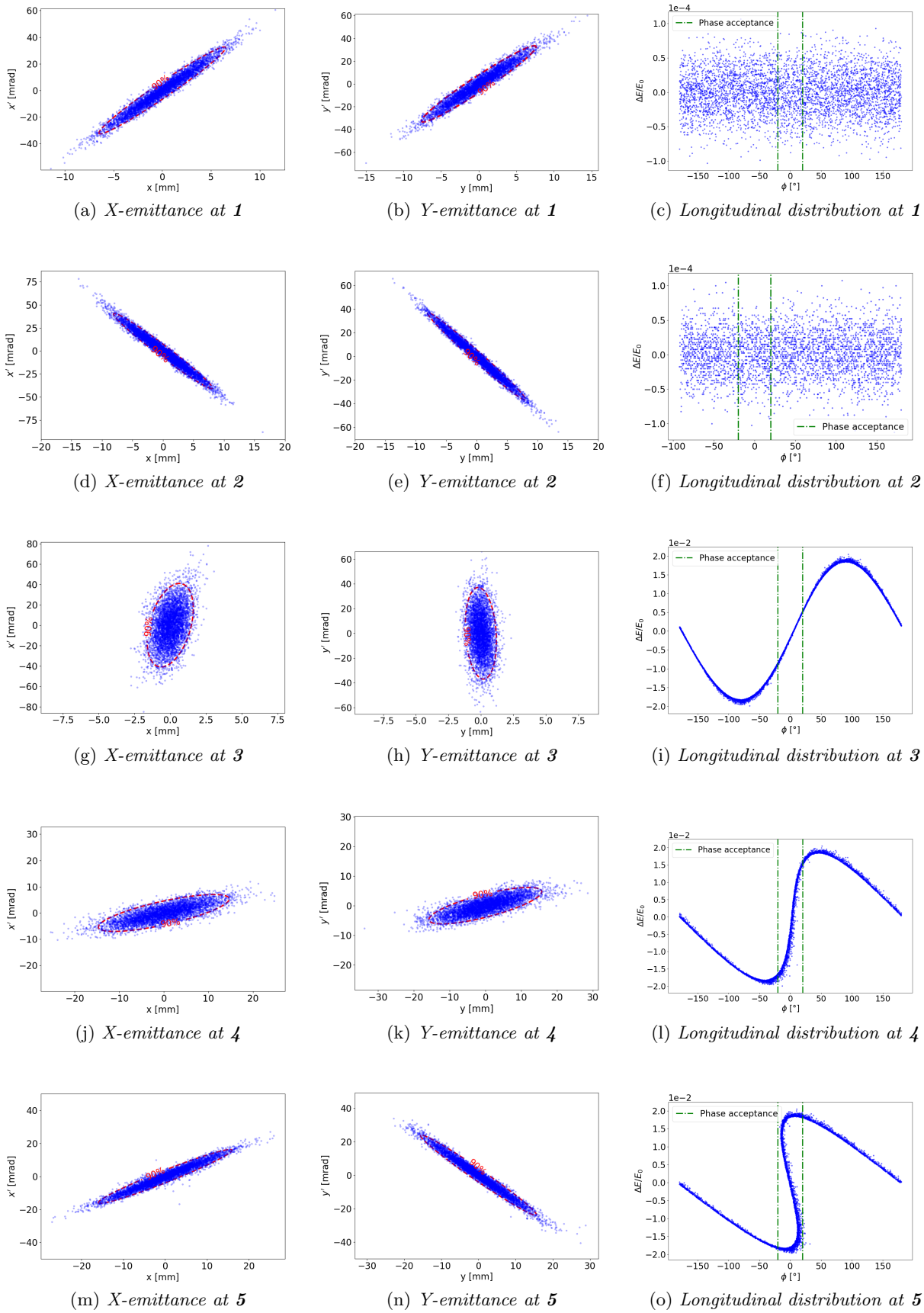

(a) *X-emittance at* ***1***
(b) *Y-emittance at* ***1***
(c) *Longitudinal distribution at* ***1***
(d) *X-emittance at* ***2***
(e) *Y-emittance at* ***2***
(f) *Longitudinal distribution at* ***2***
(g) *X-emittance at* ***3***
(h) *Y-emittance at* ***3***
(i) *Longitudinal distribution at* ***3***
(j) *X-emittance at* ***4***
(k) *Y-emittance at* ***4***
(l) *Longitudinal distribution at* ***4***
(m) *X-emittance at* ***5***
(n) *Y-emittance at* ***5***
(o) *Longitudinal distribution at* ***5***

Figure 21: Development of beam motion in the injection line, measurements are taken from points underlined in Fig. 20, for transverse emittances the 90% ellipsis are reported.

Nevertheless, this effect disappears when we introduce the other components on the injection line because it is negligible comparing to solenoids effect on the transverse dynamics that gives to the ions a significant focusing transverse momentum. Moreover, the fact that the beam does not fill the buncher diameter, but is almost concentrated near the axis, can be another reason for the irrelevance of this effect. In Tab. 9 we can see that the transverse parameters, both with a $\beta\lambda/2$ buncher and with a $\frac{3}{2}\beta\lambda$ one, are very similar to the ones without a buncher. We can conclude that in our condition an axial buncher does not influence substantially the transversal motion.

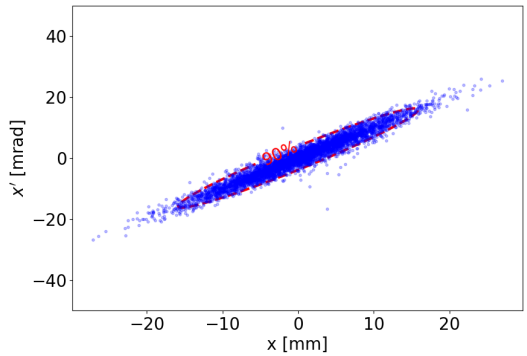

(a) *X-emittance at inflector without the buncher*

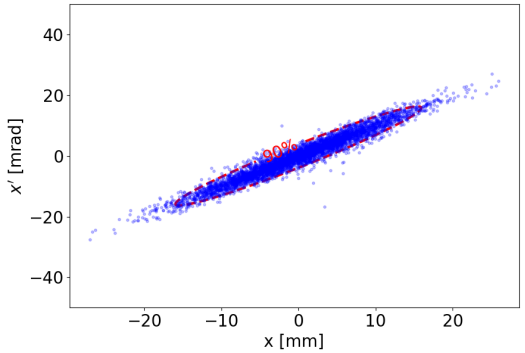

(b) *X-emittance at inflector with the $\beta\lambda/2$ buncher*

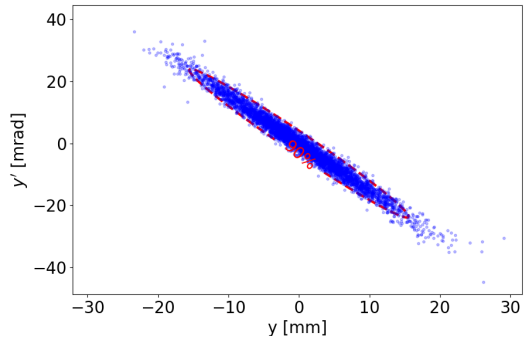

(c) *Y-emittance at inflector without the buncher*

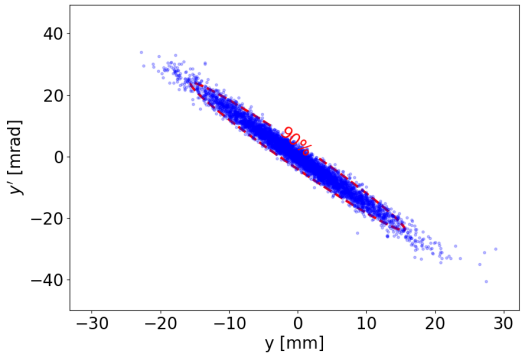

(d) *Y-emittance at inflector with the $\beta\lambda/2$ buncher*

Figure 24: Comparison between transverse emittances with and without buncher

		$\varepsilon_{90\%}$ [π·mm·mrad]	α	β [mm/mrad]	γ [mrad/mm]	R_{max} [mm]	R'_{max} [mrad]
No buncher	X	61.5	-4.1	4.1	4.3	15.6	16.3
	Y	63.2	5.8	3.8	9.1	15.5	23.9
$\beta\lambda/2$	X	62.0	-4.1	4.1	4.3	15.9	16.3
	Y	64.3	5.7	3.8	9.0	15.6	24.0
$\frac{3}{2}\beta\lambda$	X	62.9	-4.0	4.1	4.3	15.6	16.4
	Y	65.3	5.6	3.7	8.8	15.6	24.0

Table 9: Transversal emittance comparison

5.2 Longitudinal dynamics

Let us now study the longitudinal dynamics at the inflector in order to check the theoretical results exposed in chapter 4. The effect of the buncher on the longitudinal dynamics can be clearly seen in Fig. 21 looking at the pictures regarding the longitudinal distribution. Before the buncher, the phases of particles are uniformly distributed, while their energy distribution is normal ($E = 40000 \pm 1$ eV). Then the buncher introduces a strong correlation between phase and energy variables in order to concentrate the largest possible number of particles within the phase acceptance.

Various simulations are performed, with the buncher working at different voltages. Beam characteristics are measured at the inflector location ($z = 2232$ mm). In Tab. 10 we report the fraction of particle within the phase acceptance (N_{bunch}/N_{tot}) and the bunching factor $\epsilon = N_{bunch}/N_{no\ bunch}$ (where $N_{no\ bunch}$ is the number of particle within the phase acceptance at 0 V) at given voltage. The maximum energy spread $\Delta E_{max}/E_0$, where $E_0 = E = 40000$ eV, is also shown. Note that we do not use a statistic error; instead, a maximum deviation is computed. This is because the energy distribution of particles at the inflector is far from a gaussian curve. It is a bimodal distribution as can be seen in Fig. 25.

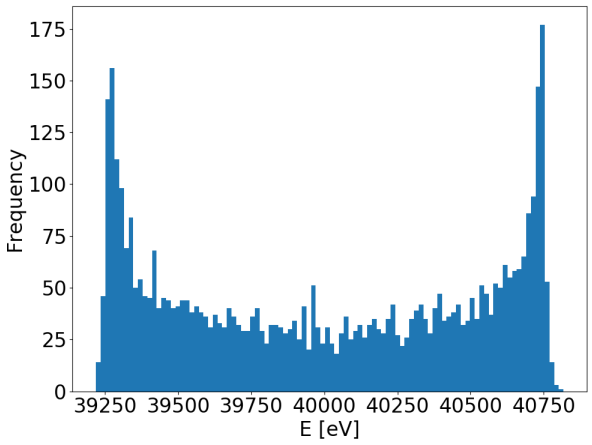

Figure 25: Energy distribution at the inflector at 800 V

V_0 [V]	ϵ	N_{bunch}/N_{tot}	$\Delta E_{max}/E_0$
0	1.0	11%	10^{-4}
600	4.1	46%	0.015
700	4.7	52%	0.018
800	5.1	57%	0.020
850	5.2	58%	0.021
900	4.4	49%	0.023
1000	3.0	33%	0.026

(a) $\beta\lambda/2$

V_0 [V]	ϵ	N_{bunch}/N_{tot}	$\Delta E_{max}/E_0$
0	1.0	11%	10^{-4}
600	4.2	46%	0.015
700	4.7	53%	0.018
800	5.2	58%	0.020
850	5.1	57%	0.022
900	4.3	48%	0.023
1000	3.0	33%	0.026

(b) $\frac{3}{2}\beta\lambda/2$

Table 10: Bunching efficiency

The simulations show that the maximum bunching effect is for a voltage of $800 \div 850$ V as we expected from the theoretical calculations. The maximum efficiency is 5 which is quite high; that means that the number of ions accelerated by the cyclotron can be five times the actual number. In Fig. 26 the bunching effect is visualized: particles are concentrated in several equidistant bunches.
Even in this analysis, there are no big differences between the two design layouts, they reach the same efficiencies at the same voltage as we expected from theory. Also the energy spread remains the same.

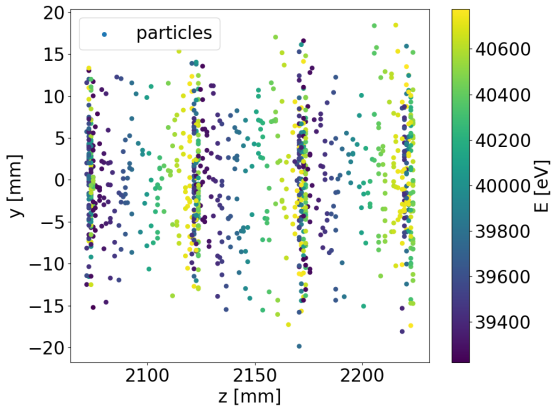

Figure 26: Space distribution of particles before the inflector

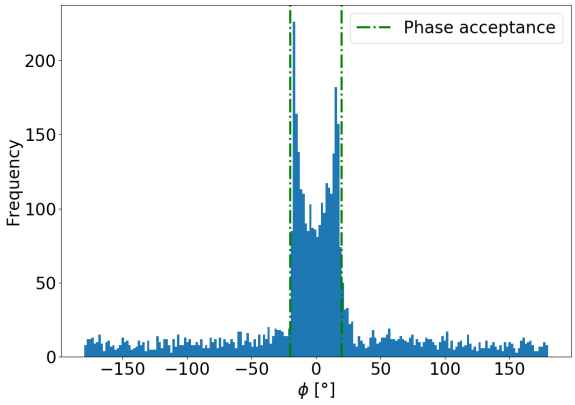

Figure 27: ϕ distribution at the inflector at 850 V

In Fig. 28 the phase-energy distributions for different choice of V_0 are reported. Note that when $V_0 = 850$ V there is the maximum concentration of particles within the acceptance as we expected after the optimization made in the Section 4.3. Also the phase distributions follows what we expect from

that Section. In particular, note in Fig. 27 how the distribution presents the two maxima typical of a $\mu > 1$ parameter as we seen in Fig. 13. In this case, in fact, $V_0 = 850$ V and $\mu = \frac{2\pi\nu L}{v}\frac{qV_0 \cdot TTF}{E} \simeq 1.58$.

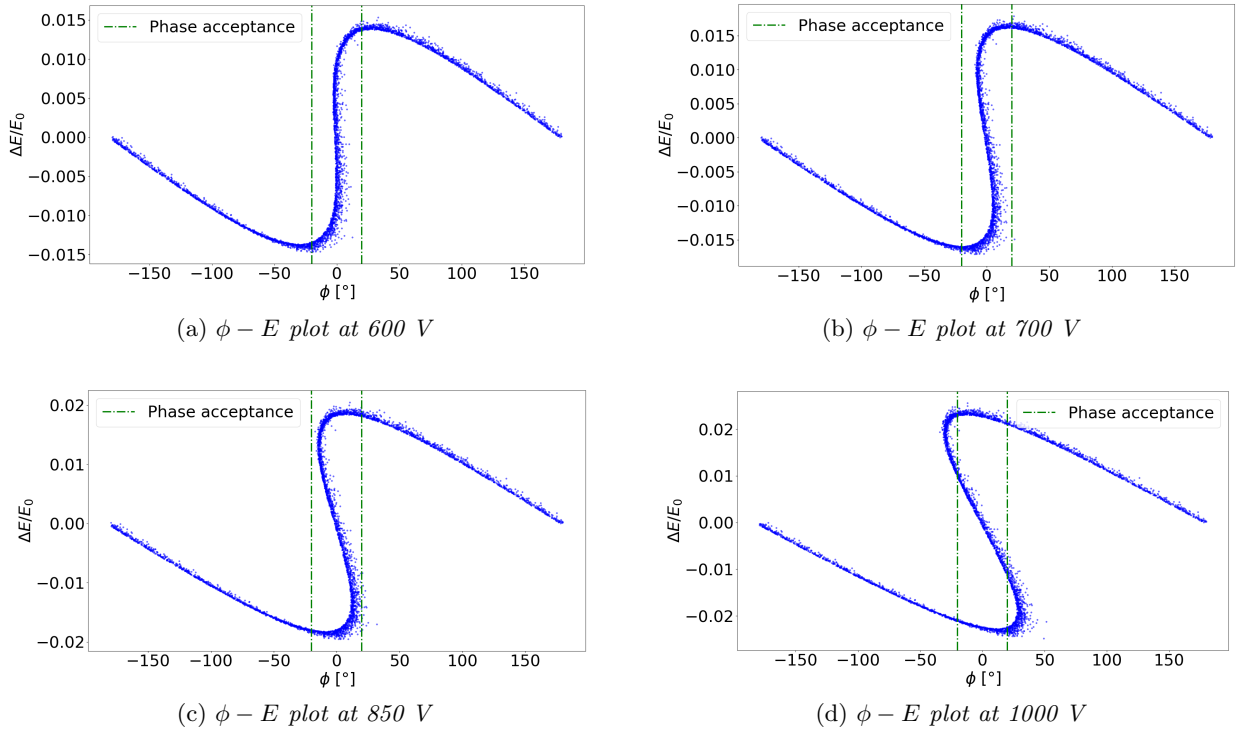

(a) $\phi - E$ *plot at 600 V*

(b) $\phi - E$ *plot at 700 V*

(c) $\phi - E$ *plot at 850 V*

(d) $\phi - E$ *plot at 1000 V*

Figure 28: Comparison among phase-energy distributions at different voltages

5.3 More harmonics

Here a quick discussion about using a waveform composed of more harmonics is presented. As it was exposed in Section 4.2 the ideal waveform for a double gap buncher, to concentrate particles within an infinitesimal phase interval, is a triangular one. A triangular waveform can be obtained adding an infinite number of sinusoidal harmonics as in the following function series:

$$F_{triangolare}(t) = \Sigma_{k=0}^{\infty}(-1)^k \frac{\sin((2k+1)\omega t)}{(2k+1)^2}$$

It is possible to feed the buncher gaps with a sum of two or three harmonics in order to approximate a triangular waveform; moreover, it is possible to find (only recursively and not analytically) the best parameters for every harmonics (See [21]). However, it is important to underline that with a simple sinusoidal waveform, we have already obtained a concentration of more than 50% of particles in our acceptance interval. As reported in Section 4.2, a triangular waveform can bunch perfectly half of the particles and not more than that. We can imagine that even by using more harmonics than the fundamental, the efficiency will not be improved considerably. That is why we choose to use an easier to produce sinusoidal potential. In Tab. 11 the comparison between the fundamental waveform and a not optimized sum of the first and third harmonics is shown. Note that the efficiency is almost the same in both cases. The effort, for what concerns costs and technical issues, of implementing a multiple harmonics oscillating system does not seem to be justified.

	ϵ	N_{bunch}/N_{tot}
fundamental	5.1	57%
1^{st} and 3^{rd}	5.0	55%

Table 11: Comparison between two different waveform at 800 V

6 Conclusion

To summarize, in the present work, beam dynamics studies were performed on the injection line of SPES cyclotron at LNL in order to develop an axial beam buncher able to improve the cyclotron performances. After the theoretical treatment of buncher generalities, we computed the specific voltage and design parameters needed for the injection line at LNL. Finally, some simulations in SIMION were run to check the theoretical results and compare the beam behaviour in the line before and after the introduction of a buncher.

We saw that an axial beam buncher can actually improve the cyclotron injection efficiency. The choice adopted is a double gap buncher (in order to halve the needed voltage) driven by a simple sinusoidal waveform. To maximize its performance the maximum voltage should be between 800 V and 850 V. In this case, we showed that there is no need of adding other harmonics to the fundamental to reach a well-shaped triangular waveform since the bunching factor is already more than 50%, which is acceptable. Therefore we will hardly obtain better results using more harmonics, while the technical challenges and costs will raise up. The maximum efficiency found is $\epsilon \simeq 5$; that means that the cyclotron will be able, in theory, to accelerate five times the particles boosted at present. We also pointed out that the introduction of a buncher does not substantially affect the transverse motion of particles; in particular at the inflector no emittance variations have been seen.

The design of the buncher was conceived to minimize the Transit Time Factor effect, and so minimize the needed voltage, without any beam loss. Two final layouts ($\beta\lambda/2$ and $\frac{3}{2}\beta\lambda$) has been presented and studied. They differ in length of the electrodes. From the beam dynamics point of view, there are no differences between them, so the final choice might be made based on technical considerations, not contemplated in this work, for example mechanical or electronic ones. A discriminant factor could be the difference between the two ground electrodes. In the $\beta\lambda/2$ buncher they are longer than in the $\frac{3}{2}\beta\lambda$ buncher, so they will avoid more significantly fringing field effects outside the buncher.

Further analysis could be done in order to improve the reliability of the results. The most important one regards the space charge effect, studying in particular the differences in dynamics among various injected currents. Another important issue is to examine the beam motion inside the inflector and the central region of the cyclotron, to understand if the introduction of a buncher could negatively affect the trajectories of the ions inside the accelerator. Finally, it will be important to deal with the description of the technical aspects of the buncher realization, including the mechanics and the electronics.

Bibliography

[1] P. Antonini, A. Lombardi, M. Maggiore, and L. Pranovi, "Design of an Injection Buncher for the SPES Cyclotron", *INFN LNL Annual Report*, p. 3, 2017.

[2] R. Baartman, "Intensity limitations in compact H cyclotrons", in *Proc. 14th Int'l Conf. on Cyclotrons and their Applications*, pp. 440–445, 1995.

[3] J. J. Livingood, *Principles of cyclic particle accelerators*. Van Nostrand, 1961.

[4] M. Maggiore, P. Antonini, A. Lombardi, L. Pranovi, and Z. Filipovski, "Review and Current Status of the 70 MeV High Intensity Proton Cyclotron at Legnaro.", Presented at the 22nd Int. Conf. on Cyclotrons and their Applications (Cyclotrons'19), Cape Town, South Africa, Sep. 2019, paper TUC01.

[5] M. Maggiore, D. Campo, P. Antonini, A. Lombardi, M. Manzolaro, A. Andrighetto, A. Monetti, D. Scarpa, J. Esposito, and L. Silvestrin, "SPES: A new cyclotron-based facility for research and applications with high-intensity beams", *Modern Physics Letters A*, vol. 32, no. 17, p. 1740010, 2017.

[6] M. Maggiore, A. Lombardi, L. Piazza, and G. Prete, "An intrinsically safe facility for forefront research and training on nuclear technologies—an example of accelerator: the SPES cyclotron", *The European Physical Journal Plus*, vol. 129, no. 4, p. 69, 2014.

[7] M. Maggiore, P. Antonini, A. Lombardi, L. Pranovi, and L. Buriola, "Status of SPES Cyclotron", *INFN LNL Annual Report*, p. 212, 2019.

[8] V. Sabaiduc *et al.*, "BEST 70P Cyclotron Factory Test.", in *Proc. 6th Int. Particle Acceleration Conf. (IPAC'15)*, Richmond, VA, USA, May 2015, pp. 3680-3682. doi:10.18429/JACoW-IPAC2015-THPF003.

[9] N. Chauvin, "Space-Charge Effect", *arXiv preprint arXiv:1410.7991*, 2014.

[10] F. Löhl, "Measurements of the Transverse Emittance at the VUV-FEL", tech. rep., DESY, 2005.

[11] D. A. Edwards and M. J. Syphers, *An introduction to the physics of high energy accelerators*. John Wiley & Sons, 2008.

[12] M. Reiser, *Theory and Design of Charged Particle Beams*. John Wiley & Sons, 2008.

[13] M. V. Lachinov, *Design studies on the axial injection system of the CYCLONE-44 cyclotron*. PhD thesis, University of British Columbia, 1998.

[14] J. Buon, "Beam phase space and emittance", tech. rep., Paris-11 Univ., 1992.

[15] D. Campo. (private comunications).

[16] D. Faircloth, "Ion sources for high-power hadron accelerators", *arXiv preprint arXiv:1302.3745*, 2013.

[17] J. Kim, "Numerical Simulation of a Multi-Cusp Ion Source for High Current H-Cyclotron at RISP", *Physics Procedia*, vol. 66, pp. 498–505, 2015.

[18] A. Laxdal, F. Ames, R. Baartman, W. Rawnsley, A. Sen, and V. Verzilov, "Allison Scanner Emittance D iagnostic Development at TRIUMF", *THIOC02, LINAC2014, Geneva, Switzerland*, 2014.

[19] V. Kumar, "Understanding the focusing of charged particle beams in a solenoid magnetic field", *American Journal of Physics*, vol. 77, no. 8, pp. 737–741, 2009.

[20] A. H. Scholldorf, *Beam emittance of the Stony Brook Tandem-LINAC booster*. PhD thesis, State University of New York, 1984.

[21] V. Pandit, P. Sarma, and R. Bhandari, "Optimization of the parameters of an ion beam buncher", *Nuclear Instruments and Methods in Physics Research Section A: Accelerators, Spectrometers, Detectors and Associated Equipment*, vol. 276, no. 1-2, pp. 21–24, 1989.

[22] H. Watson and J. W. Gewartowski, *Principles of Electron Tubes*. Von Nostrand, 1965.

[23] G. Dôme, "Theory of RF Acceleration and RF noise", tech. rep., CERN, 1984.

[24] W. Kleeven, W. Gelbart, and J. Sura, "Optical properties of a two-gap buncher", *Nuclear Instruments and Methods in Physics Research Section B: Beam Interactions with Materials and Atoms*, vol. 64, no. 1-4, pp. 367–370, 1992.

[25] P. Antonini, L. Buriola, A. Lombardi, M. Maggiore, and L. Pranovi, "Studies for a Buncher for the Injection System of the 70 MeV Cyclotron", *INFN LNL Annual Report*, p. 143, 2019.

[26] P. Antonini, A. Lombardi, M. Maggiore, L. Pranovi, and L. Buriola, "Buncher for the Optimization of the Injection of a 70 MeV Cyclotron.", Presented at the 22nd Int. Conf. on Cyclotrons and their Applications (Cyclotrons'19), Cape Town, South Africa, Sep. 2019, paper TUP010.